# Determination of the dispersive elastic constants of the cubic crystals Ge, Si, GaAs, and InSb

K. Jakata and A. G. Every*
*School of Physics, University of the Witwatersrand, PO Wits 2050, South Africa*
(Received 4 March 2008; revised manuscript received 9 April 2008; published 8 May 2008)

The first onset of spatial dispersion, i.e., the variation of velocity of an elastic wave when its wavelength approaches the natural scale of length of a medium, can be accommodated within continuum elasticity theory by the incorporation of third and fourth order spatial derivatives of the displacement field in the elastic wave equation. This paper is concerned with the access to the coefficients of these higher order derivatives in gradient elasticity provided by inelastic neutron scattering, ballistic phonon imaging, and picosecond laser ultrasound measurements. Numerical values of the dispersive elastic constants of the four cubic crystals, germanium, silicon, gallium arsenide, and indium antimonide, are obtained by fitting to available near zone center symmetry direction acoustic mode phonon dispersion relations of these crystals, measured by inelastic neutron scattering. Ballistic phonon transport calculations using these values, account well for available dispersive phonon images of these crystals. For Ge, Si, and GaAs, comparison is made with values of dispersion coefficients reported elsewhere in literature, which have been obtained from laser ultrasound measurements and from empirical and *ab initio* lattice dynamics models.

DOI: 10.1103/PhysRevB.77.174301 PACS number(s): 62.30.+d, 62.65.+k, 43.35.+d

## I. INTRODUCTION

The velocity of elastic waves in a solid becomes wavelength dependent when the wavelength approaches the natural scale of length of the medium, which is characterized by, e.g., the lattice spacing in a crystal or the range of the interatomic forces. This variation of velocity is known as spatial dispersion, and its first onset can be accommodated within continuum elasticity theory by the incorporation of third and fourth order spatial derivatives of the displacement field in the elastic wave equation.[1–4] This adaptation, known as gradient elasticity, has found widespread application in recent years (see, e.g., Refs. 3–7). Its advantage over detailed microscopic models tailored to specific media is its universal nature, with its mathematical form being independent of the particular microstructure giving rise to the dispersion. The limitations of gradient elasticity are that it is not applicable to wavelengths comparable to or smaller than the natural length scale and, without a large number of higher order derivatives, it does not give an accurate representation of the phonon dispersion relation near the Brillouin zone boundary of periodic structures. As regards application to wave propagation and phonon transport problems, this is not a severe drawback, since near zone boundary acoustic waves tend to be highly attenuated through scattering and anharmonic decay. Moreover, in general, their group velocities approach zero at the zone boundary, which renders them essentially nonpropagating.

The coefficients of the higher order derivatives in the wave equation constitute a set of dispersion constants. This paper is concerned with the access to the numerical values of these constants that is provided by picosecond laser ultrasound measurements,[8] dispersive phonon imaging,[9] and, either directly or indirectly through the intermediary of lattice dynamics models, phonon dispersion relations measured by inelastic neutron scattering.[10] Our investigation relates to the four cubic crystals, Ge, Si, GaAs, and InSb. For these crystals, symmetry considerations dictate that there are six independent coefficients of the fourth order derivatives, the dispersive elastic constants $f_1,\ldots,f_6$, and for the latter two crystals, which lack a center of inversion, there is, in addition, a single independent coefficient for the third order derivatives, the dispersion constant $d$. We derive values of the nondispersive and dispersive elastic constants by fitting to the known near zone center portions of the acoustic mode phonon dispersion curves for the symmetry directions of these crystals that have been obtained by neutron scattering. We find that ballistic phonon transport calculations employing these constants account well for the dispersive phonon images of these crystals. These images are an acid test of the nondispersive and dispersive elastic constants in that, unlike neutron scattering and the laser ultrasound experiments that we are aware of, they explore all crystallographic directions, not just the symmetry directions. For Ge, Si, and GaAs, there are previously reported values of dispersion constants obtained from empirical and *ab initio* lattice dynamics models and from laser ultrasound measurements, which we compare our results to.

## II. DISPERSIVE WAVE EQUATION

The first onset of spatial dispersion of acoustic waves in media with microstructure can be accommodated within continuum elasticity theory by the incorporation of third and fourth order spatial derivatives of the displacement field **u** in the wave equation as follows:[1–4]

$$\rho\frac{\partial^2 u_i}{\partial t^2} = c_{ikjl}\frac{\partial^2 u_j}{\partial x_k\,\partial x_l} + d_{ikjlm}\frac{\partial^3 u_j}{\partial x_k\,\partial x_l\,\partial x_m} + f_{ikjlmn}\frac{\partial^4 u_j}{\partial x_k\,\partial x_l\,\partial x_m\,\partial x_n} + \cdots, \tag{1}$$

where the subscripts refer to Cartesian axes, $\rho$ is the density, the coefficients of the second order derivatives, $c_{ikjl}$, are the conventional nondispersive elastic constants, and those of the third and fourth order derivatives, $d_{ikjlm}$ and $f_{ikjlmn}$, re-

 

spectively, are dispersive elastic constants. We restrict our attention to the domain of weak spatial dispersion near the Brillouin zone center, not more than about halfway to the zone boundary, where there is no need to consider higher order derivatives than those displayed in Eq. (1).

Equation (1) admits plane wave solutions of the form $u_j = U_j \exp[i(\mathbf{k}\cdot\mathbf{x}-\omega t)]$, with the wave vector $\mathbf{k}$, angular frequency $\omega$, and polarization vector $\mathbf{U}$ satisfying the following linear equation:

$$\{D_{ij} - \rho\omega^2\delta_{ij}\}U_j = 0, \tag{2}$$

where

$$D_{ij} = c_{ikjl}k_k k_l + id_{ikjlm}k_k k_l k_m - f_{ikjlmn}k_k k_l k_m k_n \tag{3}$$

is the dynamical matrix. The secular equation,

$$\Omega(\mathbf{k},\omega) = \det|D_{ij} - \rho\omega^2\delta_{ij}| = 0, \tag{4}$$

represents the dispersion relation for elastic waves in the medium.

For crystals of cubic symmetry, the elastic modulus tensor $c_{ikjl}$ has three independent components, which in the Voigt contracted notation are $c_{1111}=C_{11}$, $c_{1122}=C_{12}$, and $c_{1212}=C_{44}$. The fifth rank tensor $d_{ikjlm}$, which identically vanishes for centrosymmetric crystals, is called the acoustic gyrotropic tensor and is implicated in the phenomenon of acoustic activity[11] in certain noncentrosymmetric crystals. For the centrosymmetric crystal class $O_h$, to which Ge and Si belong, $d_{ikjlm}$ is zero, while for the crystal class $T_d$, to which GaAs and InSb belong, which lacks inversional symmetry, this tensor has a single independent component, $d_{12223}$, which we abbreviate to $d$. Symmetry considerations limit the number of independent components of the $f_{ikjlmn}$ tensor for the $O_h$ and $T_d$ classes to 6, namely, $f_1 \equiv f_{111111}$, $f_2 \equiv f_{122122}$, $f_3 \equiv f_{122133}$, $f_4 \equiv f_{211222}$, $f_5 \equiv f_{112222}$, and $f_6 \equiv f_{112233}$. In terms of these coefficients, the components of the dynamical matrix for cubic crystals are given by[1,2]

$$D_{ii} = C_{11}k_i^2 + C_{44}(k_j^2 + k_k^2) - f_1 k_i^4 - f_2(k_j^4 + k_k^4) - 6f_3 k_j^2 k_k^2 - 6f_4 k_i^2(k_j^2 + k_k^2) \tag{5}$$

and

$$D_{ij} = (C_{12} + C_{44})k_i k_j + 3id(k_i^2 k_k - k_j^2 k_k) - 4f_5(k_i k_j^3 + k_i^3 k_j) - 12f_6(k_i k_j k_k^2). \tag{6}$$

No summation is implied by repeated indices in these expressions and it is required that $i \neq j$, $j \neq k$, and $k \neq i$. Note that Refs. 1 and 2 employ symmetrized elastic constants $\tilde{c}_{ikjl}$, for which $\tilde{c}_{1122}=(C_{12}+C_{44})/2$.

For the crystals we are considering, the elastic constants $C_{ij}$ are of the order of $10^{12}$ dyn/cm$^2$. We can estimate the magnitudes of the $d$ and $f_i$ coefficients on the grounds that the terms in Eq. (6) should all be of the same order of magnitude for $k=2\pi/a$, where $a \approx 6$ Å is the lattice constant. Hence, we expect that $d \sim 10^4$ dyn/cm and $f_i \sim 10^{-4}$ dyn, which are born out in the tables that follow.

## III. EXTRACTION OF ELASTIC CONSTANTS AND DISPERSION CONSTANTS FROM NEUTRON SCATTERING DATA

Inelastic neutron scattering measurements of phonon dispersion relations are generally restricted to crystallographic symmetry directions. We have determined the numerical values of the elastic constants and dispersion constants of Ge, Si, GaAs, and InSb by fitting to measured near zone center acoustic mode frequency versus wave vector data for the ⟨100⟩, ⟨111⟩, and ⟨110⟩ crystallographic directions in these four crystals. In these directions, there is at least one pure transverse mode, and this allows the factorization of Eq. (4) into a linear factor and a quadratic factor in terms of the squared frequency and wave number. For the ⟨100⟩ and ⟨111⟩ directions, and in the case of $O_h$ symmetry, also the ⟨110⟩ direction, the quadratic factor further factorizes, which yield expressions of the form $\omega^2 = ak^2 - bk^4$, where $a$ and $b$ are constants, for the dispersion curves as follows.

For the fourfold symmetry ⟨100⟩ directions, Eqs. (4)–(6) yield the following:

$$\rho\omega_L^2 = C_{11}k^2 - f_1 k^4, \tag{7}$$

for the longitudinal mode, and

$$\rho\omega_T^2 = C_{44}k^2 - f_2 k^4, \tag{8}$$

for the doubly degenerate transverse modes.

The dispersion relation for the longitudinal mode along the threefold ⟨111⟩ directions is

$$\rho\omega_L^2 = \tfrac{1}{3}(C_{11} + 2C_{12} + 4C_{44})k^2 - \tfrac{1}{9}(f_1 + 2f_2 + 6f_3 + 12f_4 + 16f_5 + 24f_6)k^4, \tag{9}$$

and for the doubly degenerate transverse modes is

$$\rho\omega_T^2 = \tfrac{1}{3}(C_{11} - C_{12} + C_{44})k^2 - \tfrac{1}{9}(f_1 + 2f_2 + 6f_3 + 12f_4 - 8f_5 - 12f_6)k^4. \tag{10}$$

Along the ⟨110⟩ crystal axes, there is a pure transverse mode with the following dispersion relation:

$$\rho\omega_{T2}^2 = \tfrac{1}{2}(C_{11} - C_{12})k^2 - \tfrac{1}{4}(f_1 + f_2 + 6f_4 - 8f_5)k^4. \tag{11}$$

The dispersion relations for the other two modes can be expressed in the following form:

$$\rho\omega^2 = \tfrac{1}{2}(A \pm \sqrt{B}), \tag{12}$$

where

$$A = \tfrac{1}{2}(C_{11} + C_{12} + 4C_{44})k^2 - \tfrac{1}{4}(f_1 + 3f_2 + 6f_3 + 6f_4 + 8f_5)k^4 \tag{13}$$

and

$$B = \left[\tfrac{1}{2}(C_{11} + C_{12})k^2 - \tfrac{1}{4}(f_1 - f_2 - 6f_3 + 6f_4 + 8f_5)k^4\right]^2 + 9d^2k^6. \tag{14}$$

The positive sign in Eq. (12) pertains to the longitudinal mode and the negative sign to a transverse mode, and Eq. (14) shows that these modes also depend on $d^2$. For $T_d$ symmetry, the presence of the $d$ term in Eq. (6) causes these

modes to be slightly mixed and of elliptical polarization.[1] For $O_h$ crystals for which $d=0$, Eq. (12) reduces to

$$\rho\omega_L^2 = \tfrac{1}{2}(C_{11}+C_{12}+2C_{44})k^2 - \tfrac{1}{4}(f_1+f_2+6f_4+8f_5)k^4 \tag{15}$$

and

$$\rho\omega_{T1}^2 = C_{44}k^2 - \tfrac{1}{2}(f_2+3f_3)k^4, \tag{16}$$

which pertain to pure longitudinal and pure transverse modes, respectively.

The neutron scattering data used in determining the nondispersive and dispersive elastic constants was obtained from Refs. 12–16. The data utilized were only that for the acoustic modes and confined to $k$ values up to a maximum of between 0.4 and 0.57 in reduced wave vector coordinates, i.e., in units of $2\pi/a$, where $a$ is the lattice constant of the crystal, depending on the availability of data for the particular crystal and crystallographic direction. The number of data points available for each dispersion curve varied between 2 and 4. In cases where it was 2, excluding for the moment the modes depending on $d$, substitution into the relevant defining equation for that curve, Eqs. (7)–(11) and (15), or (16), yielded the values of the two coefficients, the first being a $C_{ij}$ or a combination of $C_{ij}$'s and the second being an $f_i$ or a combination of $f_i$'s. Where there were three or four data points for a particular dispersion curve, the values of those two constants were obtained from optimized fitting to those data points.

Proceeding in this way for Ge and Si, for which there were data available for all seven of the symmetry axis dispersion curves, we obtained the numerical values of seven combinations of the three independent $C_{ij}$'s and, likewise, the numerical values of seven combinations of the six independent $f_i$'s. These two overdetermined problems were solved by optimization, and a least-squares fit yielded the values for the $C_{ij}$ and $f_i$ of Ge and Si, as shown in Tables I and II, respectively. The $C_{ij}$'s obtained in this way differ by only a few percent from tabulated values of Landolt-Börnstein (LB),[17] which have been obtained by averaging over reported measured values. Dispersion curves for Ge and Si, calculated with these parameters and compared with the utilized neutron scattering data, are shown respectively in Figs. 1 and 2.

Table I also lists values of elastic constants and dispersion constants for Ge reported by Maranganti and Sharma,[2] which have been derived from shell model calculations of the lattice dynamics of Ge, with parameters adjusted to fit neutron scattering data for all of the branches. We have found that with these constants, we do not obtain as good a fit to the acoustic mode neutron scattering data as that shown in Fig. 1. The reason for this may be that because the shell model is simultaneously fitted to experimental data for both the optical and acoustic branches, it is therefore in a sense a compromise. Another factor may be that the dispersion constants of Maranganti and Sharma[2] apply to asymptotically small wave vector values, whereas the constants we have extracted from neutron scattering acoustic mode data have been optimized to give the best average fit to the neutron scattering data over a finite range of $k$. We were not able to locate any calculations of the $f_i$'s based on the bond charge (BC) model, which for covalent crystals such as Ge and Si are able to fit the neutron scattering data with fewer parameters.[18] The $\gamma$ coefficients in the tables and their calculated values[8,19] are explained in due course.

TABLE I. Elastic constants and dispersion constants of Ge directly extracted from neutron scattering data of Nilsson and Nelin (Ref. 12), taking the density $\rho=5.36$ g/cm$^3$ and lattice constant $a=5.65$ Å. Also shown are values of these constants obtained though the medium of the shell model by Maranganti and Sharma (Ref. 2), and dispersion constants $\gamma$ obtained from picosecond laser ultrasonic experiments of Hao and Maris (Ref. 8) and BC model calculations (Refs. 8 and 19). Also shown are the LB (Ref. 17) tabulated values of $C_{ij}$.

| | This paper | Shell model[a] | LB[b] | |
|---|---|---|---|---|
| $C_{11}(\times 10^{12}$ dyn/cm$^2)$ | 1.391 | 1.31 | 1.29 | |
| $C_{44}$ | 0.698 | 0.68 | 0.671 | |
| $C_{12}$ | 0.56 | 0.30 | 0.48 | |
| $f_1(\times 10^{-4}$ dyn) | 0.803 | 0.08 | | |
| $f_2$ | 1.506 | 2.52 | | |
| $f_3$ | 0.008 | 0.63 | | |
| $f_4$ | 0.489 | 0.03 | | |
| $f_5$ | 0.439 | 0.01 | | |
| $f_6$ | −0.320 | −0.29 | | |
| | | | Ultrasound[c] | BC[cd] |
| $\gamma_{\langle 100\rangle}(\times 10^{-11}$ cm$^3$/s) | 1.47 | 0.15 | 0.85 | 1.50 |
| $\gamma_{\langle 110\rangle}$ | 3.66 | 1.27 | 5.55 | 5.52 |
| $\gamma_{\langle 111\rangle}$ | 1.64 | 0.48 | 1.05 | 2.46 |

[a]Reference 2.
[b]Reference 17.
[c]Reference 8.
[d]Reference 19.

In Table II, the elastic constants and dispersion constants of Si, directly extracted from neutron scattering data, are compared with values that have been obtained through the medium of *ab initio* lattice dynamics, molecular dynamics, and the shell model by Maranganti and Sharma. [2] As with Ge, and probably for the same reasons, these other values of the constants do not yield as good a fit to the acoustic mode neutron scattering data as that shown in Fig. 2, which is based on the neutron scattering constants.

For InSb and GaAs, for which the parameter $d$ is nonzero, the dispersion relations for the quasilongitudinal and quasitransverse modes in the $\langle 110\rangle$ direction take on the more complicated form described by Eq. (12), while the expressions for the other five dispersion curves, being independent of $d$, are unaffected. From the $\langle 100\rangle$ and $\langle 111\rangle$ data, we have obtained the $C_{ij}$ values for these two crystals, but determining the $f_i$ has presented somewhat more of a challenge. We attempted to approximate Eq. (12) by polynomial expressions of the same form as the other dispersion relations through a power series expansion of the surd, but this was not successful in fitting the dispersion relations out as far as we would have liked. The reason for this could be traced to

TABLE II. Elastic constants and dispersion constants of Si directly extracted from the neutron scattering data of Dolling (Ref. 13) and Nilsson and Nelin (Ref. 14), taking the density $\rho=2.33$ g/cm$^3$ and lattice constant $a=5.43$ Å. Also shown are values of these constants obtained though the medium of the shell model, molecular dynamics and *ab initio* lattice dynamics by Maranganti and Sharma (Ref. 2), and dispersion constants $\gamma$ obtained from picosecond laser ultrasonic experiments of Hao and Maris (Ref. 8) and BC model calculations (Refs. 8 and 19), and Landolt-Börnstein (Ref. 17) tabulated values of $C_{ij}$.

| | This paper | Molecular dynamics[a] | *Ab initio* LD[a] | Shell model[a] | LB[b] | |
|---|---|---|---|---|---|---|
| $C_{11}(\times 10^{12}$ dyn/cm$^2)$ | 1.775 | 1.45 | 1.68 | 1.66 | 1.65 | |
| $C_{44}$ | 0.807 | 0.70 | 0.81 | 0.80 | 0.791 | |
| $C_{12}$ | 0.745 | 0.84 | 0.45 | 0.48 | 0.63 | |
| $f_1(\times 10^{-4}$ dyn) | 0.752 | 0.37 | 2.9 | 0.39 | | |
| $f_2$ | 1.25 | 0.27 | 4.1 | 2.7 | | |
| $f_3$ | −0.013 | −0.19 | −0.42 | 0.48 | | |
| $f_4$ | 0.524 | 0.34 | 0.84 | 0.48 | | |
| $f_5$ | 0.378 | 0.32 | 0.67 | 0.06 | | |
| $f_6$ | −0.125 | −0.10 | −0.66 | −0.24 | | |
| | | | | | Ultrasound[c] | BC[c,d] |
| $\gamma_{\langle 100\rangle}(\times 10^{-11}$ cm$^3$/s) | 1.85 | 1.01 | 7.33 | 0.99 | 1.80 | 2.20 |
| $\gamma_{\langle 110\rangle}$ | 4.65 | 3.16 | 10.40 | 3.86 | 8.45 | 8.00 |
| $\gamma_{\langle 111\rangle}$ | 3.09 | 1.70 | 3.54 | 2.52 | 2.60 | 3.52 |

[a]Reference 2.
[b]Reference 17.
[c]Reference 8.
[d]Reference 19.

the comparable magnitude of certain terms of different powers in the discriminant for the larger values of $k$. For extracting the parameters $f_i$ and $d$ from neutron scattering data, there is an advantage in being able to work with expressions that are combinations of terms in $k^2$ and $k^4$, and we have obtained these from Eq. (12) by combining the longitudinal mode and fast transverse mode expressions as follows:

$$\rho\omega_L^2 + \rho\omega_{T1}^2 = A, \tag{17}$$

and

$$(\rho\omega_L^2 - \rho\omega_{T1}^2)^2 = B. \tag{18}$$

From Eqs. (13) and (14), $A$ has the desired form, while $B$ in addition contains a term in $k^6$, which we have neglected.

For GaAs, neutron scattering data[15] were available for all seven symmetry direction dispersion curves and might have been sufficient to determine all of the seven dispersion constants except that a singular valued problem arises from the fact that the coefficient of $k^4$ in Eq. (17) is a linear combination of the coefficients of $k^4$ in Eqs. (7)–(11). The solution of this underdetermined optimization problem was a line segment of points in dispersion parameter space, which we parametrized by $d^2$, which had a lower limit of zero and an

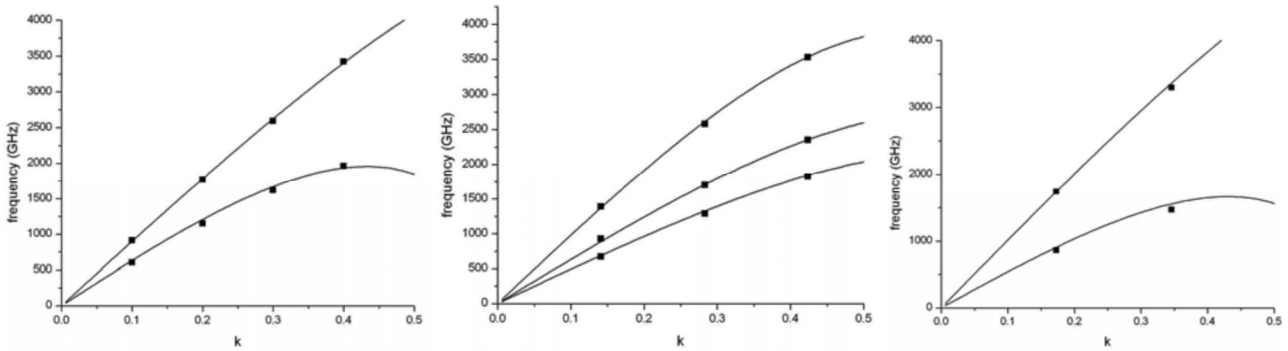


FIG. 1. Dispersion curves (frequency $\omega/2\pi$ versus reduced wave vector $k$) of Ge along the (a) ⟨100⟩, (b) ⟨110⟩, and (c) ⟨111⟩ crystallographic directions using elastic constants and dispersion constants directly extracted from neutron scattering data. The data points represent the neutron scattering data of Nilsson and Nelin (Ref. 12).

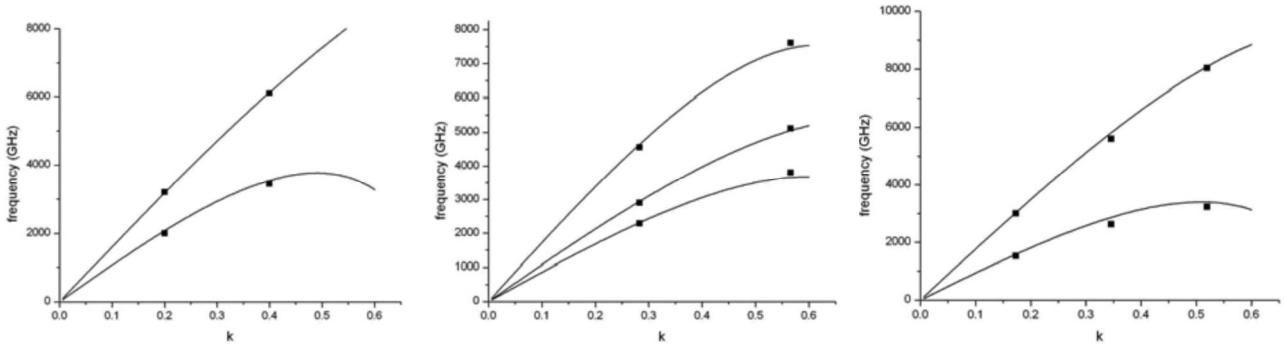


FIG. 2. Dispersion curves of Si along the (a) ⟨100⟩, (b) ⟨110⟩, and (c) ⟨111⟩ directions using nondispersive and dispersive elastic constants directly extracted from neutron scattering data. The data points represent the neutron scattering data of Dolling (Ref. 13) and Nilsson and Nelin (Ref. 14).

upper limit beyond which one or more of the $f_i$ became imaginary. The value of $d^2$ was narrowed down within that interval to that which gave the best visual fit to all of the neutron scattering data we exploited. The elastic constants and dispersive constants of GaAs obtained by these means are shown in Table III, alongside values obtained through the medium of the shell model, dipole model, and *ab initio* lattice dynamics by Maranganti and Sharma[2] and DiVincenzo,[1] and elastic constants from LB.[17]

The dispersion curves of GaAs shown in Fig. 3 have been calculated by using elastic constants directly extracted from neutron scattering data. The data points in the dispersion curves represent the experimental neutron scattering data of Dolling and Waugh.[15] Again, we find that with the lattice dynamics derived constants, we do not obtain as good a fit to the acoustic mode neutron scattering data as that shown in Fig. 3.

The nondispersive and dispersive elastic constants of InSb were determined in a similar way to that of GaAs, except that we were not able to exploit the dispersion relation for the pure transverse mode in the ⟨110⟩ direction, since no neutron scattering data are available for that branch for InSb. This

TABLE III. Elastic constants and dispersion constants of GaAs directly extracted from the neutron scattering data of Dolling and Waugh (Ref. 15), taking the density $\rho=5.34$ g/cm$^3$ and lattice constant $a=5.65$ Å. Also shown are values of these constants obtained through the medium of the shell model, dipole model, and *ab initio* lattice dynamics by Maranganti and Sharma (Ref. 2) and DiVincenzo (Ref. 1), dispersion constants $\gamma$ obtained from picosecond laser ultrasonic experiments of Hao and Maris (Ref. 8) and BC model calculations (Refs. 8 and 19), and Landolt-Börnstein (Ref. 17) tabulated values of $C_{ij}$.

| | This paper | Dipole model[a] | *Ab initio* LD[a] | Shell model[b] | LB[c] | |
|---|---|---|---|---|---|---|
| $C_{11}(\times 10^{12}$ dyn/cm$^2)$ | 1.200 | 1.190 | 1.170 | 1.200 | 1.18 | |
| $C_{44}$ | 0.580 | 0.600 | 0.560 | 0.600 | 0.594 | |
| $C_{12}$ | 0.576 | 0.540 | 0.620 | 0.540 | 0.535 | |
| $f_1(\times 10^{-4}$ dyn) | 0.400 | 0.40 | 0.40 | 0.26 | | |
| $f_2$ | 0.900 | 1.05 | 1.08 | 2.04 | | |
| $f_3$ | −0.093 | 0.45 | 0.94 | 0.48 | | |
| $f_4$ | 0.357 | 0.25 | 0.22 | 0.24 | | |
| $f_5$ | 0.280 | 0.03 | 0.24 | 0.16 | | |
| $f_6$ | −0.200 | −0.08 | 0.02 | −0.19 | | |
| $d(\times 10^4$ dyn/cm) | 0.25 | 0.41 | 0.13 | 0.18 | | |
| | | | | | Ultrasound[d] | BC[de] |
| $\gamma_{\langle 100\rangle}(\times 10^{-11}$ cm$^3$/s) | 0.79 | 0.79 | 0.80 | 0.51 | 0.74 | 1.34 |
| $\gamma_{\langle 110\rangle}$ | 2.54 | 1.42 | 2.12 | 2.24 | 8.15 | 4.44 |
| $\gamma_{\langle 111\rangle}$ | 1.08 | 1.29 | 2.74 | 1.56 | 1.20 | 2.28 |

[a]Reference 2.
[b]Reference 1.
[c]Reference 17.
[d]Reference 8.
[e]Reference 19.

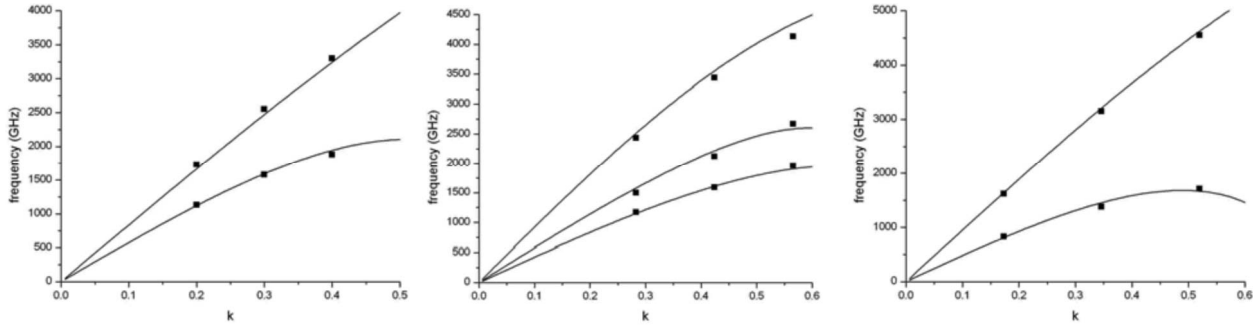


FIG. 3. Dispersion curves of GaAs along the (a) ⟨100⟩, (b) ⟨110⟩, and (c) ⟨111⟩ directions using values of the elastic constants directly derived from neutron scattering data. The data points represent the neutron scattering data of Dolling and Waugh (Ref. 15).

posed an underdetermined problem of six independent equations for seven parameters, which yielded, as with GaAs, a line segment of points in parameter space. We chose the point on this line which yields dispersion curves along the direction through the center of the irreducible sector of the Brillouin zone (polar and azimuthal angles with respect to the cube axes $\theta=32°$ and $\varphi=47°$, respectively), which lie well within the bounds represented by the symmetry direction dispersion curves. The elastic constants and dispersion constants of InSb obtained in this way are shown in Table IV, and dispersion curves for the ⟨100⟩, ⟨110⟩, and ⟨111⟩ directions, calculated by using these constants, are shown in Fig. 4 together with data points representing the experimental neutron scattering data of Price *et al.*[16] These curves show good agreement with experimental data except for the pure $T$ mode in the ⟨110⟩ direction, for which there are no data.

## IV. PICOSECOND LASER ULTRASOUND MEASUREMENTS OF DISPERSION

Hao and Maris[8] carried out laser ultrasound measurements on a number of crystals that provide a window on the onset of spatial dispersion for the longitudinal modes in the symmetry directions of these crystals. In their experiments, a picosecond laser pulse momentarily heats the aluminum coated surface of their sample, which generates a pressure pulse of short duration that propagates through the sample, is reflected off the opposite face, and has its return to the first surface monitored. The acoustic pulse has a peak frequency of about 120 GHz, and it represents a coherent excitation that allows for the accurate measurement of dispersion in this frequency domain. In its passage through the crystal, the pulse spreads out into an oscillatory Airy function type wave form, with the higher spatial frequency Fourier components of the pulse lagging behind the lower frequency leading edge because of dispersion. Hao and Maris were able to fit their results to a dispersion relation of the following form:[8]

$$\omega(k) = Vk - \gamma k^3 \ldots , \tag{19}$$

where $V$ is the longitudinal velocity in the long wavelength limit and the coefficient $\gamma$ is a dispersion parameter. By comparing Eq. (19) to the dispersion relation (7), we see that for the ⟨100⟩ direction,

$$V_{\langle 100\rangle} = \sqrt{C_{11}/\rho}; \quad \gamma_{\langle 100\rangle} = \frac{V_{\langle 100\rangle} f_1}{2C_{11}}. \tag{20}$$

From Eqs. (9) and (15), similar expressions hold for the ⟨111⟩ and ⟨110⟩ symmetry directions, with the coefficients of $k^2$ and $k^4$ in these equations replacing $C_{11}$ and $f_1$ in Eq. (20), respectively. For the ⟨110⟩ direction in GaAs, where $d$ is nonzero, we have evaluated $\gamma_{\langle 110\rangle}$ by expanding the surd in Eq. (12) in powers of $k^2$ and by extracting the coefficients of $k^2$ and $k^4$. Because of the smallness of $k$ here, there was no

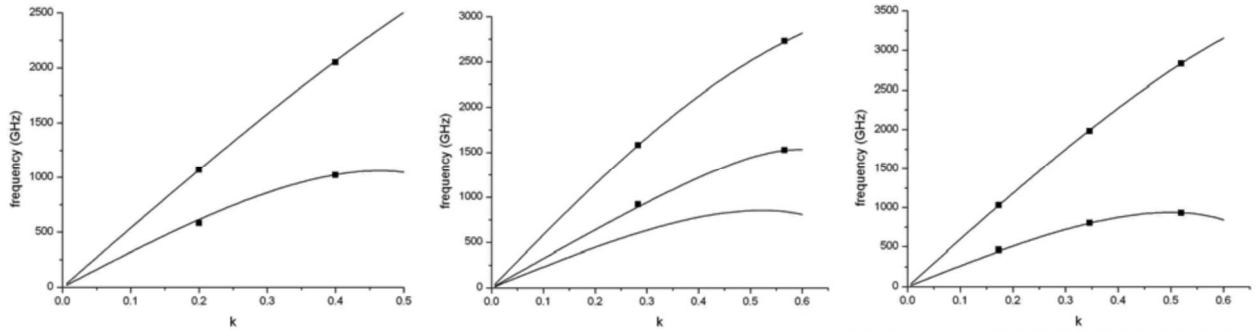


FIG. 4. Dispersion curves of InSb along the (a) ⟨100⟩, (b) ⟨110⟩, and (c) ⟨111⟩ directions. The data points represent the neutron scattering data of Price *et al.* (Ref. 16).

TABLE IV. Nondispersive and dispersive elastic constants of InSb directly extracted from neutron scattering data of Price *et al.* (Ref. 16), taking density $\rho=5.79$ g/cm$^3$ and lattice parameter $a=6.48$ Å. Also shown are the Landolt-Börnstein (Ref. 17) tabulated values of $C_{ij}$.

| | This paper | LB[a] |
|---|---|---|
| $C_{11}(\times 10^{12}$ dyn/cm$^2)$ | 0.707 | 0.662 |
| $C_{44}$ | 0.252 | 0.302 |
| $C_{12}$ | 0.449 | 0.359 |
| $f_1(\times 10^{-4}$ dyn) | 0.4162 | |
| $f_2$ | 0.6181 | |
| $f_3$ | −0.2103 | |
| $f_4$ | 0.2964 | |
| $f_5$ | 0.2258 | |
| $f_6$ | −0.0924 | |
| $d(\times 10^4$ dyn/cm) | 2.000 | |

[a]Reference 17.

recurrence of the problem encountered before.

In Table I, the values of the dispersion parameters $\gamma$ of Ge reported by Hao and Maris[8] are compared with those calculated by using Eq. (20) and equivalent equations for the other directions, using the nondispersive and dispersive elastic constants derived from neutron scattering data and those derived through the medium of the shell model, and the BC model of Weber.[8,19] Although these four sets of values appreciably differ, the neutron scattering, laser ultrasound, and BC values bear the best comparison. A point of consistency between all four sets of values is that $\gamma_{\langle 110\rangle}$ has the largest value, $\gamma_{\langle 100\rangle}$ the smallest, and $\gamma_{\langle 111\rangle}$ the intermediate value. The laser ultrasound measurements are indicative of a larger variation of $\gamma$ with direction than the neutron scattering data.

In Table II, the values of the dispersion parameters $\gamma$ of Si reported by Hao and Maris[8] are compared with those calculated by using the constants derived from neutron scattering data and those obtained through the medium of molecular dynamics, *ab initio* lattice dynamics, the shell model, and the BC model.[8,19] The neutron scattering and laser ultrasound values of $\gamma_{\langle 100\rangle}$ and $\gamma_{\langle 111\rangle}$ are in good agreement, but as with Ge, the neutron scattering value of $\gamma_{\langle 110\rangle}$ is somewhat lower than the laser ultrasound one. The model derived results differ from both the neutron scattering and laser ultrasound ones, in the case of the *ab initio* lattice dynamics even yielding the $\gamma$'s in a different order by size. Picosecond ultrasound measurements on Si by Daly *et al.*[20] yielded $\gamma_{\langle 100\rangle}=1.44\times 10^{-11}$ cm$^3$/s and $\gamma_{\langle 111\rangle}=1.92\times 10^{-11}$ cm$^3$/s, which are slightly smaller than those of Hao and Maris.[8]

In Table III, the values of the dispersion parameters $\gamma$ of GaAs reported by Hao and Maris[8] are compared with those calculated by using the constants derived from neutron scattering data and those obtained through the medium of the dipole model, *ab initio* lattice dynamics, the shell model, and the BC model.[8,19] As with Si, the neutron scattering and laser ultrasound values of $\gamma_{\langle 100\rangle}$ and $\gamma_{\langle 111\rangle}$ are in good agreement, but the neutron scattering value of $\gamma_{\langle 110\rangle}$ is somewhat lower than the laser ultrasound one. The model derived results differ from both the neutron scattering and laser ultrasound ones, in the case of the *ab initio* lattice dynamics, yielding the $\gamma$'s in a different order by size.

We are not aware of any laser ultrasound measurements or lattice dynamics model based calculations of the dispersion constants $f_i$, $d$, and $\gamma$ of InSb.

## V. PROBING SPATIAL DISPERSION WITH PHONON IMAGING

In contrast to neutron scattering and hitherto reported laser ultrasound measurements, phonon imaging explores the effects of spatial dispersion in all directions in a crystal, not just the high symmetry directions. A phonon image depicts the highly anisotropic directional dependence of the thermal phonon flux emanating from a heated spot on the surface of a crystal.[9] The measurements are conducted at liquid helium temperatures, where there is minimal phonon scattering, and the phonon transport takes place ballistically. By raster scanning the source (usually a pulsed focused laser beam), with the detector at a fixed position on the opposite face of the crystal, a map is made from the directional dependence of the radiated phonon intensity. Bolometric detectors are most effective for measurements on longer wavelength less dispersive phonons, while frequency selective tunnel junction detectors are used for measurements on shorter wavelength dispersive phonons.[9] By far, the most important contributory factor to the nonuniformity in the phonon flux is the effect of phonon focusing, which has to do with the fact that phonons propagate not in the directions of their wave vectors $\mathbf{k}$, which are smoothly distributed in direction for a thermal source, but in the directions of their group velocity or ray vectors, $\mathbf{V}=\partial\omega(\mathbf{k})/\partial\mathbf{k}$. For a given frequency, these rays are perpendicular to the constant frequency surface and, as a result, they tend to be bunched up in directions normal to regions where the surface is flattest. Caustics in the phonon intensity arise from lines of zero curvature in the constant frequency surface.[9,21,22]

In the low frequency limit, which is reasonably well satisfied for thermal phonons up to and a little beyond 100 GHz, the constant frequency surfaces are all identical in shape to the acoustic slowness surface, which is determined just by the elastic constants $C_{ij}$, and the consequences are nondispersive phonon images, which are frequency independent, and the caustics being extremely sharp. At higher frequencies, the constant frequency surfaces change with frequency, and so do phonon focusing patterns, and the caustics undergo some blurring. There is an extensive literature on dispersive phonon focusing. In the past, the results were generally interpreted on the basis of lattice dynamics models.[23–31] The only exception to this appeared to be an attempt to explain certain anomalies in the focusing pattern of quartz near its acoustic axes on the basis of first order spatial dispersion.[32]

The phonons that feature in dispersive phonon focusing are those with wave vectors sufficiently far from the center of the Brillouin zone that they are in the nonlinear region of the dispersion relation, but not so far from the center that they are near the zone boundary where group velocities tend

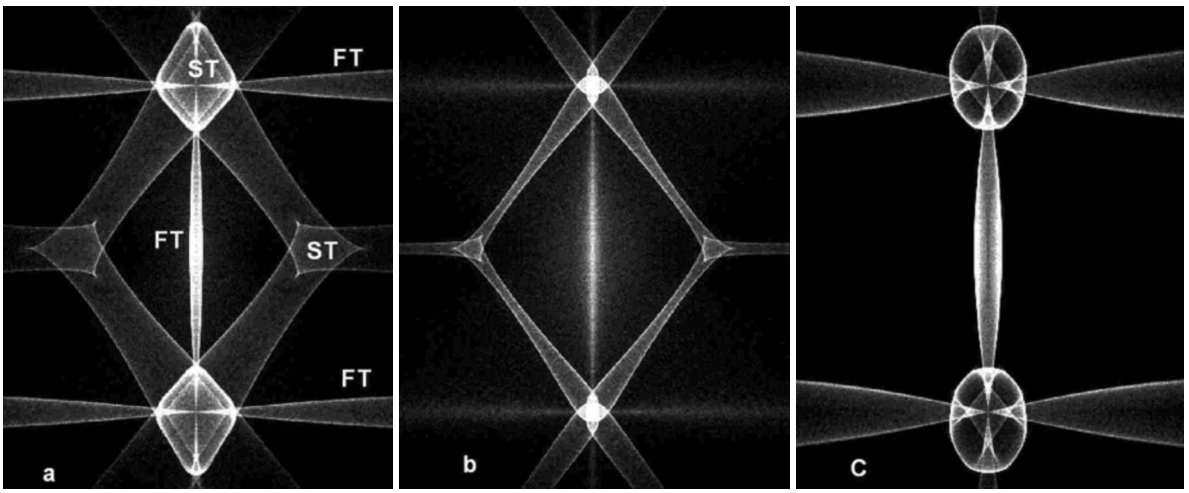


FIG. 5. Calculated phonon images of Ge in the (110) observation plane (a) for essentially nondispersive phonons using elastic constants and dispersion constants directly extracted from neutron scattering data, (b) for essentially nondispersive phonons by using elastic constants and dispersion constants derived through the medium of the shell model (Ref. 2), and (c) by using neutron scattering elastic constants and dispersion constants and selecting wave vectors $k$ up to 0.15 and phonons with frequencies near 0.85 THz.

to zero, and phonon scattering is pronounced. These are precisely the modes which our gradient elasticity model is designed for. In our numerical modeling of phonon images, we assume a three-dimensional uniform distribution of wave vectors out to a maximum value of $k \approx 0.4$. From the dispersion relation (6), which depends on $f_i$ and, where applicable, also on $d$, we calculate the frequencies and group velocities for all these **k**'s, and the points where these rays intersect the viewing surface are collected in a $500 \times 500$ array of bins, and the distribution used to simulate a phonon image. To match the experimental conditions for reported phonon images, in some cases, we select the arrivals by frequency interval and, where time gating has been employed in the measurements, also by arrival time.

Figure 5 shows three calculated phonon images of Ge in the (110) observation plane, the first two for essentially nondispersive phonons in the frequency range 0–0.3 THz, and the third for higher frequency dispersive phonons. Bright regions in these images correspond to high phonon intensity, with the sharp lines being caustics. Figure 5(a) was calculated by using elastic constants directly extracted from neutron scattering data, while Fig. 5(b) was calculated by using elastic constants derived through the medium of the shell model by Maranganti and Sharma.[2] The labels ST and FT refer to phonon focusing structures due to slow and fast transverse phonons, respectively. The first of these images is in good agreement with the phonon image measured by Northrop and Wolfe,[33] but their measured image is poorly reproduced by using elastic constants derived through the medium of the shell model, particularly with regard to the diamond shaped ST structures centered on the ⟨100⟩ directions (near the top and bottom center in the image), and the absence of fully formed FT caustics. Figure 5(c) shows an image that results from selecting phonons with frequencies at

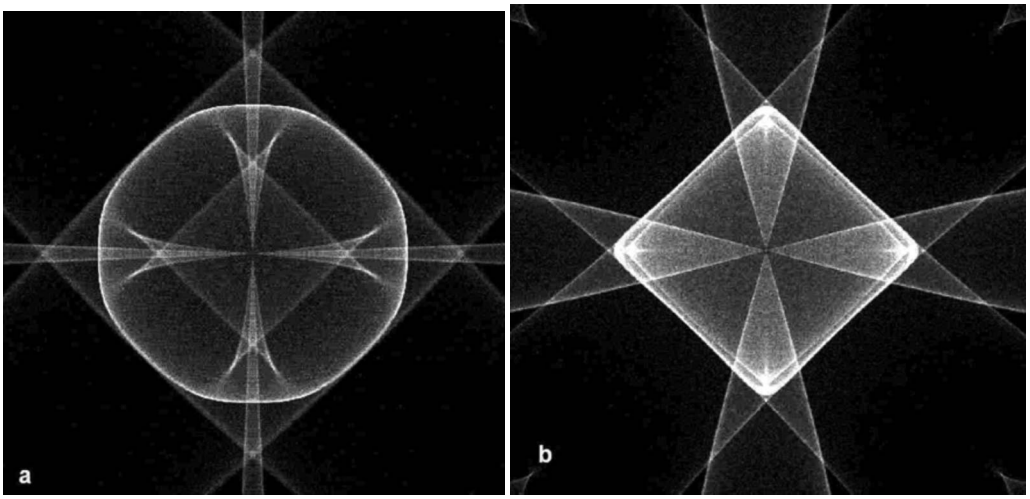


FIG. 6. Calculated phonon images of Si in the (100) observation plane for the frequency range $0.7 \leq f \leq 0.9$ THz: (a) using elastic constants and dispersion constants directly extracted from neutron scattering data and (b) using elastic constants and dispersion constants derived through the medium of molecular dynamics by Maranganti and Sharma (Ref. 2).

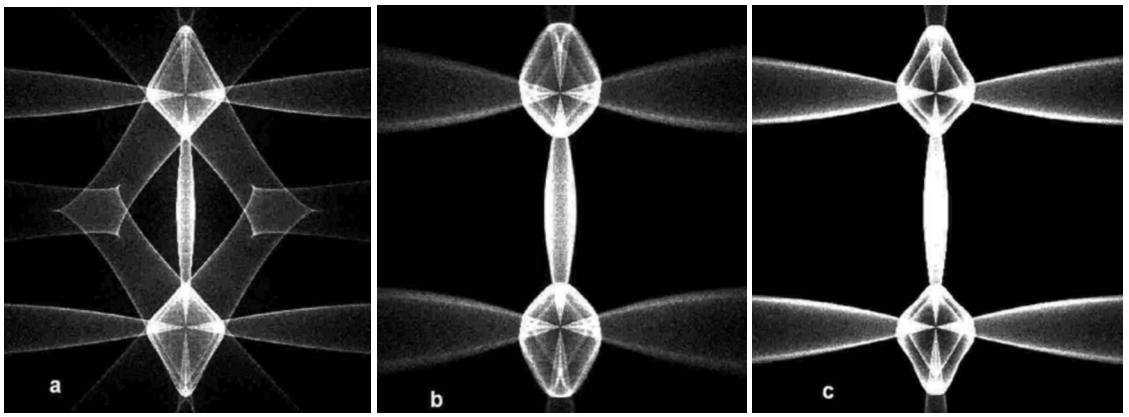


FIG. 7. Calculated phonon images of GaAs in the (110) observation plane: (a) essentially nondispersive image using neutron scattering elastic constants and dispersion constants and frequencies in the range 0–0.3 THz (the other two images are dispersive images for phonons with frequencies between 0.7 and 1.0 THz and velocities between 2.9 and 3.9 mm/$\mu$s); (b) using elastic constants and dispersion constants directly extracted from neutron scattering data; (c) using elastic constants and dispersion constants derived through the medium of the shell model by DiVincenzo (Ref. 1).

around 0.85 THz and with wave vectors up to 0.15, which are calculated by using our elastic constants and dispersion constants. This image compares well with the experimental image obtained by Dietsche *et al.*[23] and Northrop[24] using a detector with an onset frequency of 0.7 THz, particularly with regard to the rounding of the ⟨100⟩ box structures and the widening of the separation between the FT caustics. The wave vector selection results in the exclusion of phonons with smaller wavelengths, which are more susceptible to scattering, and this has the greatest effect on the three-cusped ST structures centered on the ⟨111⟩ directions, which are now suppressed. This appears to explain the absence of these focusing structures in the measured image.[23,24]

Figures 6(a) and 6(b) show dispersive phonon images of Si in the (100) observation plane, for phonons in the frequency range of 0.7–0.9 THz, calculated by using nondispersive and dispersive elastic constants directly obtained from neutron scattering data and values derived from molecular dynamics by Maranganti and Sharma,[2] respectively. The image in Fig. 6(a) compares well with the image of Si measured by Tamura *et al.*[26] using a detector with an onset frequency of 0.7 THz. The image calculated by using molecular dynamics constants for the same frequency range substantially differs from the measured image.

Nondispersive and dispersive elastic constants of GaAs directly extracted from neutron scattering data were used to calculate the long wavelength phonon image of GaAs in the (110) observation plane in Fig. 7(a). This image compares very well with the nondispersive phonon image of GaAs measured for the same geometry by Northrop *et al.*[27] and Hebboul and Wolfe.[28] Figures 7(b) and 7(c) show dispersive images of GaAs in the (110) observation plane for phonon frequencies between 0.7 and 1.0 THz, and gated to select phonons with velocities between 2.9 and 3.9 mm/$\mu$s to match the sliding time gate used in the experiments.[27] Figure 7(b) has been calculated with constants directly derived from neutron scattering data, while Fig. 7(c) is based on the shell model derived constants of DiVincenzo.[1] At these higher fre-

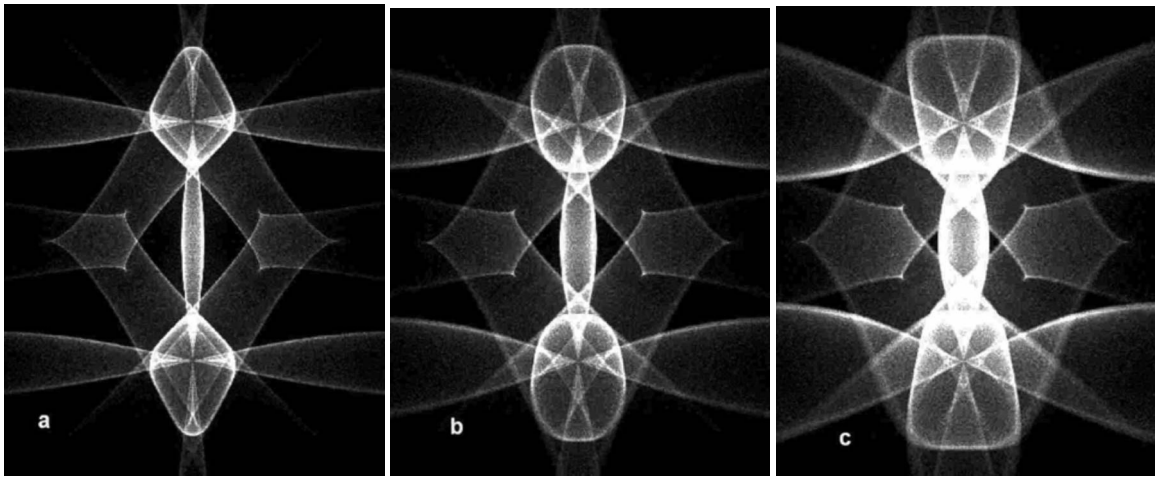


FIG. 8. Calculated phonon images of InSb in the (110) observation plane, selecting phonons with frequencies in the range (a) 0.0–0.2 THz, (b) 0.43–0.50 THz, and (c) 0.593–0.650 THz.

quencies, the diamond shaped structures around the ⟨100⟩ directions have become rounded and the separation of the FT caustics near the center of the image has increased. While both images are reasonably consistent with the experimental image,[27,28] the neutron scattering derived parameters do have the edge, with Fig. 7(b) matching up better with the measured image.

The evolution of the (110) observation plane phonon image of InSb as the phonon frequency increases is shown in Fig. 8. These images were calculated by using nondispersive and dispersive elastic constants directly extracted from neutron scattering data. The box structures around the ⟨100⟩ directions changes from a diamond shape for nondispersive frequencies [Fig. 8(a)] to a rounded shape in the 0.43–0.50 THz frequency range [Fig. 8(b)] and then becomes squared for phonons with frequencies between 0.593 and 0.650 THz [Fig. 8(c)]. The inner box structures also become smaller as a result of dispersion, and the separation of the FT caustics becomes progressively larger with increasing frequency. These changes in the phonon focusing pattern are in good agreement with the phonon images measured by Hebboul and Wolfe.[30]

## VI. CONCLUSIONS

The first onset of spatial dispersion of acoustic waves in crystals is well accounted for by augmenting the elastic wave equation with third and fourth order spatial derivatives of the displacement field. By this means, we have been able to successfully fit inelastic neutron scattering data on the phonon dispersion curves for the acoustic modes in Ge, Si, GaAs, and InSb out to about halfway to the Brillouin zone boundary. We have compared the elastic constants and dispersion constants we have obtained in this way to those calculated through the medium of lattice dynamics models by DiVicenzo[1] and Maranganti and Sharma.[2] Our values for the constants come closer to fitting the picosecond laser ultrasound measurements of spatial dispersion in the first three of these crystals by Hao and Maris.[8] With these constants, we are able to account well for the reported dispersive phonon images of the four crystals. Gradient elasticity in this context has been shown to be a useful adjunct to lattice dynamics models and an appropriate way to treat weak spatial dispersion.

## ACKNOWLEDGMENTS

J. P. Wolfe and G. Hearne are thanked for constructive suggestions. This work is based on research supported by the National Research Foundation.

*Corresponding author.
FAX: 27 11 717 6879. arthur.every@wits.ac.za

[1] D. P. DiVincenzo, Phys. Rev. B **34**, 5450 (1986).
[2] R. Maranganti and P. Sharma, Phys. Rev. Lett. **98**, 195504 (2007); J. Mech. Phys. Solids **55**, 1823 (2007).
[3] A. G. Every, Phys. Rev. B **72**, 104302 (2005).
[4] A. G. Every, J. D. Kaplunov, and G. A. Rogerson, Phys. Rev. B **74**, 184307 (2006).
[5] L. Teneketzis Tenek and E. C. Aifantis, Compos. Struct. **53**, 189 (2001).
[6] A. V. Metrikine and H. Askes, Eur. J. Mech. A/Solids **21**, 555 (2002); H. Askes and A. V. Metrikine, *ibid.* **21**, 573 (2002).
[7] M. Lazar, G. A. Maugin, and E. C. Aifantis, Int. J. Solids Struct. **43**, 1404 (2006).
[8] H.-Y. Hao and H. J. Maris, Phys. Rev. Lett. **84**, 5556 (2000); Phys. Rev. B **63**, 224301 (2001).
[9] J. P. Wolfe, *Imaging of Phonons* (Cambridge University Press, Cambridge, 1998).
[10] H. Bilz and W. Kress, *Phonon Dispersion Relations in Insulators* (Springer, Berlin, 1979).
[11] D. L. Portigal and E. Burstein, Phys. Rev. **170**, 673 (1968).
[12] G. Nilsson and G. Nelin, Phys. Rev. B **3**, 364 (1971).
[13] G. Dolling, *Inelastic Neutron Scattering* (IAEA, Vienna, 1965), Vol. 2.
[14] G. Nilsson and G. Nelin, Phys. Rev. B **6**, 3777 (1972).
[15] G. Dolling and J. L. T. Waugh, in *Lattice Dynamics*, edited by R. F. Wallis (Pergamon, London, 1965).
[16] D. L. Price, J. M. Rowe, and R. M. Nicklow, Phys. Rev. B **3**, 1268 (1971).
[17] A. G. Every and A. K. McCurdy, *Second and Higher Order Elastic Constants*, Landolt-Börnstein, New Series, Group III, Vol. 29, Pt. A (Springer, Berlin, 1992).
[18] J. P. Wolfe (private communication).
[19] W. Weber, Phys. Rev. B **15**, 4789 (1977); K. C. Rustagi and W. Weber, Solid State Commun. **18**, 673 (1976).
[20] B. C. Daly, T. B. Norris, J. Chen, and J. B. Khurgin, Phys. Rev. B **70**, 214307 (2004).
[21] H. J. Maris, in *Nonequilibrium Phonons in Nonmetallic Crystals*, edited by W. Eisenmenger and A. A. Kaplyanskii (North-Holland, Amsterdam, 1986).
[22] A. G. Every, Phys. Rev. B **24**, 3456 (1981).
[23] W. Dietsche, G. A. Northrop, and J. P. Wolfe, Phys. Rev. Lett. **47**, 660 (1981).
[24] G. A. Northrop, Phys. Rev. B **26**, 903 (1982).
[25] S. I. Tamura, Phys. Rev. B **28**, 897 (1983).
[26] S. I. Tamura, J. A. Shields, and J. P. Wolfe, Phys. Rev. B **44**, 3001 (1991).
[27] G. A. Northrop, S. E. Hebboul, and J. P. Wolfe, Phys. Rev. Lett. **55**, 95 (1985).
[28] S. E. Hebboul and J. P. Wolfe, Z. Phys. B: Condens. Matter **74**, 35 (1989).
[29] S. I. Tamura and T. Harada, Phys. Rev. B **32**, 5245 (1985).
[30] S. E. Hebboul and J. P. Wolfe, Z. Phys. B: Condens. Matter **73**, 437 (1989).
[31] K. Hayasaka, R. Higashi, J. Suda, Y. Tanaka, S. Tamura, M. Giltrow, and J. K. Wigmore, J. Phys.: Conf. Ser. **92**, 012099 (2007).
[32] A. G. Every, Phys. Rev. B **36**, 1448 (1987); A. L. Shuvalov and A. G. Every, J. Phys. A **33**, 5105 (2000).
[33] G. A. Northrop and J. P. Wolfe, Phys. Rev. B **22**, 6196 (1980).